

LINE EMISSION PROCESSES IN ATOMIC AND MOLECULAR SHOCKS

J. Michael Shull

Center for Astrophysics and Space Astronomy, and
Joint Institute for Laboratory Astrophysics
University of Colorado and National Bureau of Standards

ABSTRACT. This review discusses the observations and theoretical models of interstellar shock waves in diffuse and molecular clouds. After summarizing the relevant gas dynamics, atomic, molecular and grain processes, and physics of radiative and magnetic precursors, I describe observational diagnostics of shocks. I conclude with a discussion of two new topics: unstable or non-steady shocks and thermal conduction in metal-rich shocks.

1 INTRODUCTION

Because the physics of interstellar shock waves has recently been the subject of a comprehensive review (Shull and Draine 1987), this review will concentrate on selected aspects of shock line emission, models, and diagnostics. In particular, I will cover the basic physics of atomic shocks in diffuse clouds and multi-fluid MHD shocks with magnetic precursors, and then turn to some recent problems of non-steady shocks and the role of thermal conduction in metal-rich shocks associated with young supernova remnants.

The environments of these shocks range in density from diffuse clouds, which contain mostly atomic gas ($n_H = 0.1 - 10^3 \text{ cm}^{-3}$) and cool by optical and ultraviolet emission lines of H, He, and atomic ions, up to molecular clouds ($n(\text{H}_2) = 10^3 - 10^8 \text{ cm}^{-3}$) which cool by optical, infrared, sub-millimeter, and millimeter wavelength lines of atoms and molecules. Emission lines are widely used by astronomers as diagnostics of density, temperature, abundance, and excitation mechanism (*e.g.*, shock excitation vs. photoionization). The techniques of observation have resulted in a natural division between shocks in diffuse atomic gas and dense molecular clouds. In this review, I follow a similar division, based on the theoretical distinctions which govern diffuse and molecular shock models. In §2, I discuss single-fluid shocks in diffuse gas, the gas dynamic, atomic, molecular, and grain processes involved in their study, and the relevant observations. In §3, I discuss multi-fluid MHD shocks with magnetic precursors. In §4, I discuss two recent topics: non-steady shocks and the role of thermal conduction.

2 SINGLE-FLUID SHOCKS IN DIFFUSE CLOUDS

2.1 Gas Dynamics

A shock is sometimes described as a “hydrodynamic surprise”. A fluid element is suddenly accelerated from an initial pre-shock velocity to a post-shock velocity. Thus, shocks are supersonic disturbances driven by thermal pressure (a “piston”), radiative acceleration, or other mechanical sources. The most common sources of high velocity gas in the interstellar

medium (ISM) are supernova remnants (SNRs), stellar winds, molecular outflows from pre-main-sequence stars, and infalling H I (21-cm) clouds.

At this point, we should make an important distinction between “adiabatic” and “radiative” shock waves. The sudden, discontinuous jump in density, flow velocity, and temperature is characteristic of an adiabatic shock. No energy is lost in the front (hence the term adiabatic), and the gas is heated to a large temperature subject to the constraints of mass and momentum conservation. All single-fluid shocks contain an adiabatic shock transition. If the post-shock gas can radiate away its energy in a time short compared to the flow time, the temperature drops and the post-shock gas is compressed to maintain approximately constant total pressure – this forms the radiative shock wave. A typical compression in a strong, radiative shock, limited by magnetic pressure, is about a factor of 100. Examples of adiabatic shocks occur at the peripheries of young SNRs in the Sedov-Taylor evolution phase. The strong X-ray line emission observed toward Tycho, Kepler, and Cas A (Becker *et al.* 1979, 1980a,b) has been interpreted as shocked metal-rich ejecta (Shull 1982; Gronenschild and Mewe 1982; Hamilton, Sarazin, and Chevalier 1983). Fast non-radiative shocks, which encounter H⁰ more rapidly than it can be pre-ionized, are believed responsible for weak Balmer line emission (Chevalier and Raymond 1978; Chevalier, Kirshner, and Raymond 1980) and ultraviolet lines and two-photon continuum from filaments just outside the main optical filaments in the Cygnus Loop (Raymond *et al.* 1983; Fesen and Itoh 1985).

The structure of a “radiative shock” can approximately be divided into three regions: (1) a radiative precursor in which the ambient gas is moderately heated and partially ionized by ultraviolet photons produced in the shocked layer; (2) the “adiabatic shock front”, a thin layer in which the pre-shock gas is accelerated and heated by dissipative processes; and (3) a much broader layer, in which inelastic collisions produce radiative cooling, emission, recombination, and further compression downstream from the front. The state of the gas beyond the last layer depends on boundary conditions at the driving source and on the total column density of shocked gas. Magnetic fields, thermal conduction, and ambient UV radiation often play a role in determining the density and temperature of this interface. Recent theoretical studies of steady-state radiative shocks include Raymond (1979), Shull and McKee (1979), Seab and Shull (1983, 1985), Dopita *et al.* (1984), and Cox and Raymond (1985), while Innes, Giddings, and Falle (1987a,b,c) recently examined non-steady shocks.

The radiative precursors of fast shocks, with $V_s > 110 \text{ km s}^{-1}$, produce singly ionized H and He ahead of the front (Shull and McKee 1979). This results in a shock front in which the dissipation is governed by plasma instabilities rather than collisions, and the “collisionless shock front” has a negligible thickness. For slower shocks, the gas is only partially ionized (in the absence of external sources of ionizing radiation). The ionized component still undergoes a collisionless shock, and the large H⁰-H⁺ charge exchange cross section $\sigma_{in} = 3 \times 10^{-15} \text{ cm}^2$ (Dalgarno and Yadav 1953, Dalgarno 1958) ensures that the ions and neutrals remain coupled. The front structure in slower ($V_s < 20 \text{ km s}^{-1}$) shocks is determined by elastic H⁰-H⁰ collisions, with a scale length $\lambda_{nn} = (n\sigma_{nn})^{-1} \approx (10^{15} \text{ cm})n_0^{-1}$ set by the density of neutral particles and their elastic cross section. Since the gas “jumps” discontinuously from its pre-shock to post-shock conditions, such shocks are called “J-shocks” (Draine 1980). I will discuss multi-fluid (continuous) “C-shocks” in §3. The

existence of an adiabatic shock transition requires that the relative kinetic energies of pre-shock and post-shock gas be dissipated into heat over a scale length small compared to the cooling length. A radiative shock occurs when radiative cooling occurs faster than dynamical times. Thus, the shock velocity must be sufficiently slow or the gas sufficiently dense so that the cooling time of the post-shock gas is less than the dynamical expansion time.

The physical variables of density, velocity, pressure, and temperature behind a shock are determined by hydrodynamical equations of mass, momentum, and energy conservation for “steady flow”. (Steady flow assumes a homogeneous and steady source of pre-shock gas, as well as a shock front which does not slow appreciably in the time for gas to flow through the full cooling zone.) For quantitative analyses of radiative shocks, it is convenient to consider a frame of reference in which the adiabatic front is stationary. The pre-shock gas of density ρ_1 and pressure P_1 then flows into the front at velocity $v_1 = V_s$, is compressed discontinuously to density $\rho_2 = 4\rho_1$ (for strong shocks with $\gamma = 5/3$), decelerated to velocity $v_2 = v_1/4$, and heated to post-shock temperature $T_2 = T_s \gg T_1$. (Physical variables ahead of the front are subscripted 1, those immediately behind the front are subscripted 2, while those at general positions downstream are unsubscripted.) If a magnetic field is present (we consider the simple case of a field \vec{B} perpendicular to the flow), a sufficient level of ionization assures that B is coupled to the matter, leading to “flux freezing” in which vB and B/ρ are constant. Conservation of mass and momentum, plus the flux freezing condition, gives the downstream pressure as a function of density ρ ,

$$P(\rho) = P_1 + \rho_1 v_1^2 [1 - \rho_1/\rho] + (B_1^2/8\pi) [1 - \rho^2/\rho_1^2]. \quad (1)$$

The temperature follows from the ideal gas law, $T = [\mu P(\rho)/\rho k]$, where μ is the mean mass per particle (ions, electrons, and neutrals). Conditions immediately behind the front are derived by combining eq. (10) with the adiabatic gas law, $P/\rho^\gamma = \text{constant}$. The density jump, ρ_2/ρ_1 , at the front is then given by the solution to the quadratic equation:

$$2(2 - \gamma) \left(\frac{\rho_2}{\rho_1} \right)^2 + [(\gamma - 1)M^2 + 2\gamma(1 + \beta)] \left(\frac{\rho_2}{\rho_1} \right) - (\gamma + 1)M^2 = 0, \quad (2)$$

where we define the quantities, $c_{s1}^2 = P_1/\rho_1$; $M = v_1/c_{s1}$; and $\beta = (B_1^2/8\pi P_1)$. Here, c_{s1} is the isothermal sound speed in the pre-shock gas, $v_{A1} = B_1/(4\pi\rho_1)^{1/2}$ is the Alfvén speed, $M = (\rho_1 v_1^2/P_1)^{1/2}$ is the isothermal Mach number, and $\beta = (v_{A1}/2c_{s1})^2$ is the ratio of magnetic pressure to gas pressure. We characterize the strength of the interstellar magnetic field by the dimensionless parameter b , so that $B_1 = (10^{-6} \text{ G})n_1^{1/2}b$ and $v_A = (1.84 \text{ km s}^{-1})b$, with n_1 measured in hydrogen nuclei cm^{-3} . In interstellar clouds the parameter b is typically of order unity (Mouschovias 1976; Troland and Heiles 1986), and diffuse-cloud interstellar shocks are “super-Alfvénic” ($V_s > v_{A1}$) as well as supersonic ($V_s > c_{s1}$). In the strong-shock limit ($M \gg 1$) the Rankine-Hugoniot jump conditions reduce to:

$$\left(\frac{\rho_2}{\rho_1} \right) = \left(\frac{v_1}{v_2} \right) = \left(\frac{\gamma + 1}{\gamma - 1} \right) \rightarrow 4 \quad (3)$$

$$P_2 = \left(\frac{2\rho_1 v_1^2}{\gamma + 1} \right) \rightarrow \frac{3\rho_1 v_1^2}{4} \quad (4)$$

$$kT_2 = \left[\frac{2(\gamma - 1)}{(\gamma + 1)^2} \right] \mu_s v_1^2 \rightarrow \frac{3\mu_s v_1^2}{16}. \tag{5}$$

The last numbers are evaluated for $\gamma = 5/3$. For strong shocks ($M \gg 1, b \approx 1$) magnetic fields do not appreciably alter these jump conditions.

2.2 Shock Structure

Models of radiative shocks are usually parameterized by several quantities: the shock velocity V_s ; the pre-shock density n_1 , temperature T_1 , and magnetic field B_1 ; and the set of elemental abundances (*e.g.*, H, He, C, N, O, Ne, Mg, Si, S, Fe). The pre-shock ionization states of these elements are also required, but in the absence of external ionizing radiation, these may be specified self-consistently by computing the structure of the radiative precursor (Shull and McKee 1979). A new ingredient to shock models (Seab and Shull 1983, 1985) is a pre-shock grain model, specifying constituents and size distributions of grains and the initial depletions of the heavy elements which compose them, primarily C, O, Si, Mg, and Fe.

In steady, plane-parallel flow, one assumes $\partial/\partial t = \partial/\partial x = 0$, so that $(d/dt) = v(d/dx) = (\rho_1 v_1/\rho)(d/dx)$ is the Lagrangian derivative following a parcel of fluid. The post-shock density in the cooling zone is derived from an energy equation,

$$\frac{d}{dx} \left[\rho v \left(\frac{v^2}{2} + U + \frac{P}{\rho} \right) + \left(\frac{B^2 v}{4\pi} \right) \right] + n^2 \mathcal{L}(T) = 0. \tag{6}$$

Here, the total (specific) internal energy U includes internal quantum states of excitation. The total loss function (cooling minus heating) is given by,

$$n^2 \mathcal{L}(T) = n^2 (\mathcal{L}_{rad} + \mathcal{L}_{dis}) - H_{ext} + \sum_j n_j \left[n_e (\alpha_j E_{r,j} + C_j I_j) - 4\pi \int_{\nu_j}^{\infty} \sigma_j(\nu) (1 - \nu_j/\nu) J_\nu d\nu \right], \tag{7}$$

where \mathcal{L}_{rad} and \mathcal{L}_{dis} are the cooling rate coefficients for collisionally excited radiative transitions and molecular dissociations, and H_{ext} is any external heating source. For species (j) of density n_j , including all ion states of all elements and molecules, α_j is the recombination rate coefficient for ion state $(j + 1) \rightarrow j$. The mean energy of recombining electrons is $E_{r,j}$, the collisional ionization rate coefficient is C_j , the radiation intensity is J_ν , the ionization threshold is $I_j = h\nu_j$, and $\sigma_j(\nu)$ is the photoionization cross section. The ionization state and cooling rate behind radiative shocks are far from equilibrium, and $\mathcal{L}(T)$ differs from the radiative cooling coefficient $\Lambda(T)$.

Downstream from the shock front, radiative cooling results in a large compression ($\rho \gg \rho_1$), while the total pressure ($P + \rho v^2 + B^2/8\pi$) remains constant. For no magnetic field, the thermal pressure P varies by only 33%, from its post-shock value of $3\rho_1 v_1^2/4$ to the full value of the “ram pressure” $\rho_1 v_1^2$ when $\rho \gg \rho_1$ (eq. [1]). When $B = 0$, the final compression of the shock can be quite large,

$$\left(\frac{\rho_f}{\rho_1} \right) = M^2 \left(\frac{T_1}{T_f} \right), \tag{8}$$

where ρ_f and T_f are the final density and temperature and M is the isothermal Mach number. However, the compression is limited by a realistic initial magnetic field (eq. [12]), since the magnetic pressure eventually dominates the momentum flux ($B^2 \propto \rho^2$, whereas $P \propto \rho T$ and $\rho v^2 \propto \rho^{-1}$). Thus, the maximum compression in a strong magnetized shock is set by the relation $\rho_1 v_1^2 \approx B_f^2/8\pi = (B_1^2/8\pi)(\rho_f/\rho_1)^2$, or

$$\left(\frac{\rho_f}{\rho_1}\right) = \left(\frac{8\pi\rho_1 v_1^2}{B_1^2}\right)^{1/2} = 2^{1/2} \left(\frac{v_1}{v_{A1}}\right) \approx (77) \left(\frac{v_{s7}}{b}\right), \quad (9)$$

where $v_{s7} = (V_s/100 \text{ km s}^{-1})$, where $b \approx 1$ is the magnetic field parameter, and ρ_f and B_f are final (maximum) values of post-shock density and magnetic field. A typical compression is about a factor of 100.

2.3 Atomic and Grain Processes

The post-shock structure of radiative shocks depends on a variety of atomic processes, the most important of which are collisional ionization, photoionization, radiative and dielectronic recombination, ion charge exchange with H^0 and He^0 , and radiative cooling. The emissivity in lines and continuum is dominated by electron-impact excitation of resonance, semi-forbidden, and forbidden lines of H^0 , He^0 , He^+ and ions of abundant elements (mostly C and O ions). The rates of these processes are temperature dependent and involve heavy element abundances, gas-grain interactions, and radiative transfer.

Immediately behind an adiabatic shock of $V_s = (100 \text{ km s}^{-1})v_{s7}$, the temperature is $T_s = (3\mu_s V_s^2/16k) = (1.44 \times 10^5 \text{ K})v_{s7}^2$, where we have assumed that $\text{He}/\text{H} = 0.1$ and that H and He are singly ionized by the radiative precursor ($\mu_s = 0.636m_H$). At these temperatures, the radiative cooling is dominated by collisional ionization of He^+ and excitation of permitted and semi-forbidden lines of He^+ ($\lambda 304$) and carbon and oxygen ions. In general, the degree of ionization of these species is lower than it would be in coronal ionization equilibrium, and the initial radiative cooling rate exceeds equilibrium values by factors of 10 to 100.

The non-equilibrium ionization fractions, $f_i = n_i/n_{tot}$, of the elements are determined by integrating time-dependent differential equations of the form,

$$\left(\frac{df_i}{dt}\right) = f_{i-1}[n_e C_{i-1} + G_{i-1}] - f_i[n_e(C_i + \alpha_{i-1}) + n(H^0)Z_i + G_i] + f_{i+1}[n_e \alpha_i + n(H^0)Z_{i+1}], \quad (10)$$

where $C_i(T)$, $\alpha_i(T)$, and $Z_i(T)$ are rate coefficients ($\text{cm}^3 \text{ s}^{-1}$) for collisional ionization *from*, recombination *to*, and charge exchange *from* ionization state (i), and G_i is the photoionization rate (s^{-1}) from state (i). The coefficient $C_i(T)$ is dominated by electron impact and includes both direct (valence shell) ionization as well as autoionization following inner-shell excitation. The latter is particularly important at high temperatures for ions with 1 or 2 electrons outside a closed shell. The recombination coefficients $\alpha_i(T)$ include both radiative and dielectronic recombination; dielectronic recombination dominates over radiative by a substantial factor at high temperatures ($T > 20,000 \text{ K}$ for most ions). Tables of $\alpha_i(T)$ and $C_i(T)$ may be found in Shull and Van Steenberg (1982).

Photoionization cross sections may be found in Reilman and Manson (1979) and Clark *et al.* (1985). Charge exchange collisions with H^0 (and sometimes He^0) are often the most effective means of reducing the ion state in shocks containing a substantial population of neutrals (Shull and McKee 1979; Butler and Raymond 1980). Charge exchange of H^0 with multiply ionized species dominates dielectronic recombination when the neutral fraction $n(H^0)/n(H_{tot})$ exceeds 1 to 5%. Charge exchange rate coefficients are discussed by Dalgarno and Butler (1978), McCarroll and Valiron (1976), Butler and Dalgarno 1980; Heil, Butler, and Dalgarno (1980), Butler, Heil and Dalgarno (1980), Baliunas and Butler (1980), and Dalgarno, Heil, and Butler (1981). Generally, the rates with ions of charge $z \geq +3$ are fast ($> 10^{-9} \text{ cm}^3 \text{ s}^{-1}$). Rates for doubly charged ions are mixed: C III, S III, and Ne III are slow ($\sim 10^{-12} \text{ cm}^3 \text{ s}^{-1}$), while N III, O III, and Si III are fast. Charge exchange of N II is slow ($\sim 10^{-12} \text{ cm}^3 \text{ s}^{-1}$), but resonant charge exchange between O II and H I effectively couples the O and H ionization fractions, $(O \text{ II}/O \text{ I}) \approx (8/9)(H \text{ II}/H \text{ I})$.

Electron collisions dominate the excitation of the permitted, semi-forbidden, and optical forbidden lines of atoms and ions. Infrared fine structure lines are excited by collisions with electrons, H^+ and H^0 (Dalgarno and McCray 1972). The electron impact excitation rate coefficient $C_{ij}(\text{cm}^3 \text{ s}^{-1})$, for a transition (i-j) of energy E_{ij} , is parameterized by the dimensionless "collision strength" Ω_{ij} :

$$C_{ij} = (8.616 \times 10^{-6} \text{ cm}^3 \text{ s}^{-1}) \left(\frac{\Omega_{ij}}{g_i} \right) T^{-1/2} \exp \left(\frac{-E_{ij}}{kT} \right), \quad (11)$$

where g_i is the statistical weight of the lower state and T is the temperature (K). References for excitation of H^0 , He^0 , and He^+ and ions of heavy elements are found in Shull and McKee (1979). Other recent tabulations of collision strengths include: Osterbrock (1974, with revisions), Raymond and Smith (1977), Shull (1981), and Cox and Raymond (1985). Compilations of electron impact excitation data for atomic ions are available as scientific reports from Los Alamos (Merts *et al.* 1980) and JILA (Gallagher and Pradhan 1985).

Figure 1 shows the temperature profiles in three 100 km s^{-1} shock models (Seab and Shull 1985). The post-shock column density, N_H , is a convenient measure of post-shock distance or Lagrangian flow time, independent of pre-shock density n_1 . By the constancy of mass flux (or $n\nu$) in one-dimensional flow, $N_H = n_1 V_s t$, where t is the flow time for a parcel of fluid to reach column N_H . The three cooling profiles in Fig. 1 represent models in which heavy elements are: (i) depleted from gas phase; (ii) initially depleted, but allowed to re-enter gas phase via grain processing; and (iii) fully in gas phase (undepleted). Evidently, the post-shock abundance of atomic coolants such as C, O, Si and Fe, can have an important effect on the total column and thus the strengths of emission lines.

Grain processing in shocks comes from grain-grain collisions and thermal and non-thermal gas-grain sputtering (more details are found in Seab 1987). Modeling is complicated by the need to specify the grain constituents and size distribution, uncertainties in the sputtering yields in He-grain collisions (Barlow 1978; Draine and Salpeter 1979), and the rates of vaporization, partial vaporization, and shattering in grain-grain collisions (Seab and Shull 1983, 1985; McKee *et al.* 1987). In fast shocks ($V_s > 150 \text{ km s}^{-1}$) grain collisions with hot post-shock ions (primarily He) dominate the sputtering of small grains, whereas grain-grain collisions and non-thermal sputtering are relatively more important

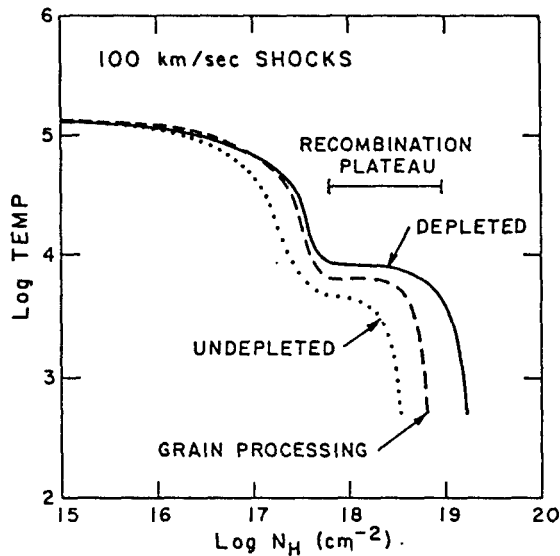


Figure 1: Post-shock temperature profiles versus column density $N_H = n_0 V_s t$ (cm^{-2}).

for larger grains in lower velocity shocks. Crucial to these “non-thermal” processes are the large gyrovelocities of charged grains generated by “betatron acceleration” as the magnetic field is compressed with the gas in the cooling zone. Most of the non-thermal grain destruction is produced in the strongly cooling layers around 10^4 K.

As the gas recombines and cools, the radiative cooling rate falls and the temperature reaches a plateau near 6000 K. Here, ionizing photons produced in the hot post-shock layer deposit their energy by photoionizing the newly recombined H^0 and He^0 . The cooling immediately behind the front is due primarily to electron-impact collisional ionization of H^0 , He^0 , or He^+ , depending on shock velocity, plus electron-impact excitation of resonance and semi-forbidden lines of H^0 ($L\gamma\alpha$), He^0 ($\lambda 584, 626$), He^+ ($\lambda 304$), and ions of abundant heavy elements, primarily C and O. Below 20,000 K, the cooling is dominated by forbidden and semi-forbidden lines of heavy elements, such as $[\text{O III}] \lambda 5007$, $[\text{O II}] \lambda 3727$, $[\text{C III}] \lambda 1909$, $[\text{S II}] \lambda 6716, 6731$ and $[\text{C II}] \lambda 2326$. Because a forbidden line may be collisionally de-excited when the electron density exceeds the line’s “critical density”, $n_{cr} = A_{21}/C_{21}$ ranging from 10^2 to 10^6 cm^{-3} , the cooling scale may be lengthened in shocks of higher density. In the gas below 10^3 K, infrared fine structure lines dominate the cooling – for example $[\text{Si II}] 34.8 \mu\text{m}$, $[\text{O I}] 63$ and $145 \mu\text{m}$, and various lines of $[\text{Fe II}]$ (1.27, 1.6, 5.0, and $26 \mu\text{m}$). If the gas contains a fraction of H_2 , the rotational lines are also important coolants.

2.4 Molecular Processes

A full discussion of molecular chemistry in diffuse clouds is beyond the scope of this paper. Useful reviews on related subjects are: molecular abundances in hydrostatic cloud models

(van Dishoeck and Black 1986), chemistry in molecular shocks (Hollenbach and McKee 1979; McKee and Hollenbach 1980), and a general review of interstellar molecular hydrogen (Shull and Beckwith 1982). Here we confine our discussion to the processes of H_2 formation and destruction. Because radiative association of two H atoms is forbidden by dipole selection rules, interstellar H_2 is believed to form most rapidly on grain surfaces. When two H^0 atoms collide with a grain and stick, they migrate and eject an H_2 molecule with substantial kinetic, vibrational, and rotational energy (Hollenbach and Salpeter 1971). In grain-free or pre-galactic environments, H_2 may also form by slower gas-phase reactions with H^- or H_2^+ (Lepp and Shull 1984; MacLow and Shull 1986; Shapiro and Kang 1987).

Dissociation of H_2 occurs either by a two-step process initiated by absorption of a UV photon in one of the Lyman ($\lambda < 1120\text{\AA}$) or Werner bands ($\lambda < 1021\text{\AA}$) or by collisions with H^0 , H^+ , or e^- (Hollenbach and McKee 1980). The photodissociation rate may be diminished by “self-shielding” in the Lyman lines (Jura 1974; Shull 1978) or by dust opacity. At low density ($n_{\text{H}} < 10^5 \text{ cm}^{-3}$) the rate of collisional dissociation can also be reduced by “radiative stabilization” (Roberge and Dalgarno 1982; Lepp and Shull 1983), in which radiative decays decrease the populations of vibrationally and rotationally excited H_2 levels which are subject to large collisional dissociation rates in thermal (Boltzmann) populations. Rate coefficients for radiative decay of vibrational and rotational states of H_2 are given by Turner, Kirby-Docken, and Dalgarno (1977), and for H^0 - H_2 collisional excitation and dissociation by Lepp and Shull (1983), revised at high temperature by MacLow and Shull (1986).

Molecular cooling in shocks arises from the excitation of rotational and vibrational states of H_2 , CO, H_2O , and other abundant molecules. Since molecular shocks are often slower and the gas denser and more neutral than in diffuse clouds, the excitation comes from collisions with H^0 and H_2 as well as from electrons. In addition, magnetic fields and multi-fluid effects play an important role (see §3). Here, we restrict our discussion to J-shocks with velocities of order 10 km s^{-1} , in which the post-shock temperature is $T_s \approx (2900\text{K})(V_s/10 \text{ km s}^{-1})^2$. These temperatures are sufficient to excite many rotational states (J) and several ($v = 1$ and 2) vibrational states of H_2 . For small J and v , the H_2 excitation temperatures are $T_e(J) = E(J)/k = (85\text{K})J(J+1)$ and $T_e(v) = (6300\text{K})v$.

2.5 Observations and Line Diagnostics

Many authors have remarked on the spectral signatures of shock waves, as distinguished from H II regions and other photoionized regions (Baldwin, Phillips, and Terlevich 1981; Fesen, Blair, and Kirshner 1985). Generally, SNRs are characterized by strong optical forbidden line emission over a wide range of ionization states. For example, $[\text{S II}]/\text{H}\alpha$ is stronger in SNRs than in H II regions. The main observational features attributed to radiative shock waves in the optical are:

1. Strong emission lines, relative to $\text{H}\beta$, of underionized species, *e.g.*, $[\text{O I}] 6300$, $[\text{N I}] 5200$, $[\text{O II}] 3726, 3729$, $[\text{S II}] 6716, 6731$.
2. A high excitation temperature ($T > 20,000$; K) measured from the intensity ratio of $[\text{O III}]$ lines, $[4363/(5007 + 4959)]$.
3. The presence of a range of ionization states, *e.g.*, $[\text{O I}]$, $[\text{O II}]$, $[\text{O III}]$, $[\text{Ne III}]$, $[\text{Ne V}]$.

4. Large ratios of [O I]/H β and [O II]/H β , relative to H II regions.

The fourth effect has been demonstrated empirically for SNRs in the Galaxy and M31/M33 (Fesen *et al.* 1985). New wavelength bands have opened up other shock discriminants. In the ultraviolet, shocks waves produce strong resonance and semi-forbidden lines of C II] 2326, C III] 1909, O III] 1663, N III] 1750, O IV] 1402, C IV 1549, and N V 1240. In the infrared, the fine structure lines of [O I] 63 μm , [Si II] 34.8 μm , [Ne II] 12.8 μm , and [Fe II] (26, 1.6, 1.27, 5 μm) are strong. While these features are not unique (photoionized gas at high densities can mimic some of the optical line ratios), the combination of lines from several ion stages and varying excitation temperatures can be used to attribute the power source to shocks.

Certain line ratios can be used to constrain the shock velocity V_s , the pre-shock density n_0 , and the abundances. The emission lines of [O III], [Ne III], C III], C IV, and N V are the best “speedometers” since their intensities rise steeply with V_s . The temperature in the post-shock “recombination zone” may be gauged by the intensity ratios of [O III] [4363/(5007+4959)] or [Ne III] 3342/3869. Density sensitive line ratios include [O II] 3729/3726 and [S II] 6716/6731, as well as certain infrared fine structure lines. Shocks into diffuse clouds generally have recombination-zone densities less than 10^3 cm^{-3} . The reason for the absence of higher densities is clear: shocks which propagate from a lower density intercloud medium into a dense cloud are slowed by a factor equal to the square root of the density contrast (momentum flux ρv^2 is conserved). The emission from these much slower shocks ($V_s = 10 \text{ km s}^{-1}$) would prove difficult to detect optically, although infrared lines of [O I], [Ne II], [Si II], and [Fe II] might be detected with a new generation of detectors.

Abundance determinations from emission lines are fraught with uncertainties. For example: (1) Changes in heavy element abundance are difficult to distinguish from differences in density, magnetic field, and velocity. (2) Intensities of strong forbidden lines “saturate” with increasing velocity or abundance, since there is only a fixed amount of energy available for these cooling lines in the recombination zone. (3) Strong UV lines such as C III] 1909 and C IV 1549 become insensitive to V_s as the post-shock temperature rises above their ionization and excitation temperature. (4) Many resonance lines (C II 1035, 1335; C IV 1549) become optically thick, and their emergent intensities are reduced by scattering in the shock layer. (5) Grain disruption by sputtering and grain-grain collisions introduces another degree of freedom: variable gas-phase abundances of C, O, Si, and Fe; (6) the shocks may be unstable or non-steady. Despite these uncertainties, one may still make progress with carefully chosen forbidden and semi-forbidden lines of ionized species (Raymond *et al.* 1981; Raymond 1984; Dopita *et al.*, 1984).

The Cygnus Loop is the best studied of the older SNRs. It is generally pictured (Raymond 1984; Hester and Cox 1986) as a 400 km s^{-1} blast wave, propagating in an intercloud medium of density $n_H \approx 0.2 \text{ cm}^{-3}$ and driving 100 km s^{-1} shocks into clouds of density $2 - 10 \text{ cm}^{-3}$. The faster, non-radiative shocks produce the observed X-rays while the slower (radiative) shocks produce the bright optical filaments. Spectra of several bright filaments show line ratios which disagree radically with radiative shock models having normal abundances and full recombination zones. Some filaments show [O III]/H β as large as 10-25, whereas current shock models do not allow ratios greater than 3, owing to rapid O $^{+2}$ - H 0 charge exchange in the recombination zone (see Table I). More generally,

Fesen *et al.* (1982) showed that the distribution of line ratios, *e.g.*, [O III]/H β versus [O II]/H β or [O II]/H β versus [O I]/H β , bears little resemblance to those predicted by standard radiative shock models.

The remedy to this disagreement may be to “truncate” the shocks’ recombination zones. A full radiative shock, complete with recombination zone, requires a column density $N_{rec} \approx 10^{19} \text{ cm}^{-2}$, corresponding to a flow time of $(3 \times 10^4 \text{ yr})(1 \text{ cm}^{-3}/n_0)(100 \text{ km s}^{-1}/V_s)$. If the zone with $T < 10^4 \text{ K}$ is missing, as a result of an inhomogeneous pre-shock medium or thermal instability, then the region which produces H β recombination lines will be missing and the O III charge exchange will be insignificant in the more ionized gas. A physical realization of this scenario for the optical filaments requires either many small ($< 10^{16} \text{ cm}$) cloudlets engulfed by the blast wave (Fesen, Blair, and Kirshner 1982), or variations in line-of-sight surface brightness produced by a few wavy thin sheets (Hester and Cox 1986; Hester 1987).

A final observational topic concerns grain destruction by shocks. Emission lines from Si and Fe are particularly affected by the grain sputtering and grain-grain collisions in the cooling zone. Seab and Shull (1983) discussed effects on the UV selective extinction curves of shock processed gas, and McKee *et al.* (1987) have recently addressed the question of “grain history”, coupling theoretical shock models of grain processing with models of the multi-phase structure of the ISM.

The *Copernicus* satellite found that significant fractions of many heavy elements are depleted from the interstellar gas, presumably locked up in dust grains. Quantitatively, we define the “depletion factor” d_i of an element (i) by,

$$\log d_i = \log \left(\frac{N_i}{N_H} \right) - \log \left(\frac{N_i}{N_H} \right)_{\odot} \quad (12)$$

where N_i and N_H are the column densities of (i) and of hydrogen, and where $(N_i/N_H)_{\odot}$ is the solar or cosmic abundance (Withbroe 1971; Grevesse 1983). The influence of shocks is believed to explain the correlation of refractory element depletions with cloud velocity. The optical observation (Routly and Spitzer 1952; Siluk and Silk 1974) that interstellar clouds with high velocities show systematically higher ratios of Ca II/Na I has been interpreted as evidence of selective grain destruction, which returns the highly depleted calcium back to gas phase. The same correlation of depletion with cloud velocity has been seen in UV absorption studies of Si and Fe (Shull, York, and Hobbs 1977). Both data and theoretical models are consistent with the general conclusion that clouds with velocities greater than about 20 km s^{-1} have larger gas-phase abundances of refractory elements than low-velocity gas. Grain processing may also be responsible for the correlation (Fig. 2) of heavy element depletions with mean line-of-sight column density $\bar{n} = N(\text{H})/\tau$. A possible physical interpretation is that lines of sight with low \bar{n} are more likely to have had extensive shock processing of grains.

3 MHD SHOCKS WITH MAGNETIC PRECURSORS

The fundamental concept underlying the following discussion of MHD shocks in gas of low fractional ionization is that the matter in the shocked regions may be thought of as consisting of several distinct, interpenetrating fluids. Normally one thinks of three fluids:

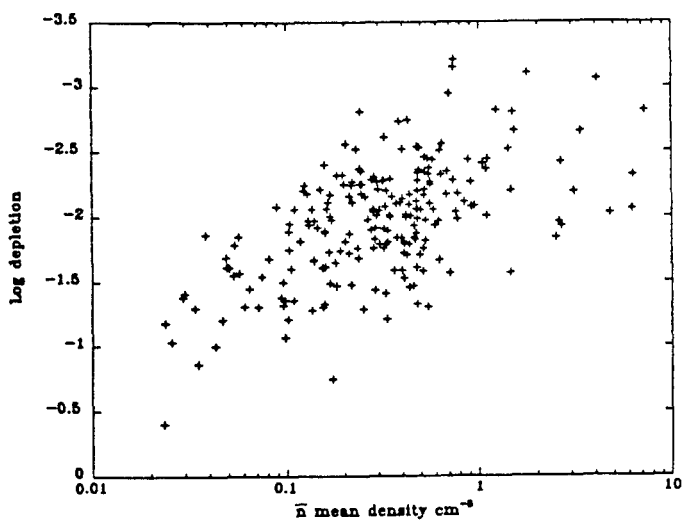


Figure 2: Depletion factors d_i for interstellar Fe toward 225 OB stars observed by IUE (Van Steenberg and Shull 1987) are correlated with mean hydrogen density \bar{n} . This effect may result from shock destruction of grains along low- \bar{n} lines of sight.

(i) the neutral particles; (ii) the ions; and (iii) the electrons. Under some circumstances it may be useful to consider the charged dust grains to constitute a fourth fluid. The motivation for this conceptual decomposition is that under some circumstances (*e.g.*, in a shock transition) these fluids may develop appreciably different flow velocities and temperatures.

A necessary condition for a shock wave to occur in an initially quiescent medium is that a compressive disturbance be advancing into the medium at a velocity greater than the signal speed. Otherwise signals will travel ahead of the shock and inform the quiescent medium that a compression is approaching. In a fluid consisting of neutrals, ions, and electrons, a wave of sufficiently long wavelength (low frequency) must have the neutrals, ions, and electrons moving together. If no magnetic field is present, the compressional signal speed is just the sound speed $c_{s, nie} = (5P/3\rho)^{1/2}$ where $P = k(n_n T_n + n_i T_i + n_e T_e)$ is the total gas pressure, and ρ is the total density. In a magnetized fluid there are two distinct compressional modes, referred to as the “fast” and “slow” magnetosonic modes; the speed v_f of the fast mode may be derived (Spitzer 1962) from the Alfvén speed $v_{A, ie} = B/(4\pi\rho_i)$ and the thermal sound speed $c_{s, ie} = [5k(n_i T_i + n_e T_e)/3\rho_i]^{1/2}$. A shock will occur if the compressive disturbance is advancing with a velocity $V_s > v_{f, nie}$.

How large are the Alfvén velocities? Existing observations of interstellar magnetic field strengths (Troland and Heiles 1986) are consistent with an empirical “scaling law” $B = (1\mu G)(n_H/\text{cm}^{-3})^{1/2}$ for densities $10\text{ cm}^{-3} < n_H < 10^6\text{ cm}^{-3}$. This relation implies relatively large values of $v_{A, ie}$ in predominantly neutral clouds containing heavy ions of

mass $\sim 20m_H$:

$$v_{A,ie} \approx (50 \text{ km s}^{-1}) \left[\frac{n_i/n_H}{10^{-4}} \right]^{-1/2} \left[\frac{20m_H}{\rho_i/n_i} \right]^{1/2}. \quad (13)$$

For example, a dense molecular cloud with $n_i/n_H = 10^{-7}$ would have $c_s \approx 1 \text{ km s}^{-1}$ and $v_{f,nie} \approx v_{A,ie} \approx 1500 \text{ km s}^{-1}$. Compressive disturbances with $V_s > v_{f,nie}$ will be shock waves, since long-wavelength signals cannot travel faster than the disturbance. More complete discussions of MHD shocks may be found in a recent review (Shull and Draine 1987) and in the literature (Draine, Roberge, and Dalgarno 1983; Draine 1986; Chernoff 1987).

Consider MHD shocks for which $V_s < v_{A,ie}$, so that the magnetized plasma is “submagnetosonic”. There are two basic classes of solutions: (1) C-type (“continuous”) shocks, and (2) J-type (“jump”) shocks with magnetic precursors. In C-type shocks, no discontinuity is present: all the flow variables vary continuously through the shock transition, and ordinary molecular viscosity plays no role. The J-type shocks resemble single fluid shocks in that there is a “jump” transition in which molecular viscosity effects an irreversible change in the neutral flow variables on a length of order one molecular mean free path; for our purposes such a change is treated as a discontinuity, with the flow variables across the discontinuity related through the Rankine-Hugoniot jump conditions. However, ahead of this “J-front” the neutral gas is accelerated and heated by collisions with streaming ions – *i.e.*, the shock has a “magnetic precursor”. In the frame of reference of the shock, the neutral gas is flowing supersonically upstream from the shock, and subsonically immediately downstream from the shock.

The dominant processes for cooling the neutral gas in C-type MHD shocks include emission from rotationally- and vibrationally-excited H_2 , rotationally excited CO, rotationally excited H_2O , and the excited fine structure levels of C I, C II, and O I. When the neutral gas temperature and density are high enough (Lepp and Shull 1983), collisional dissociation of H_2 can become an important sink for thermal energy. The electron gas can become significantly hotter than the neutrals. The electrons are cooled by elastic collisions with the neutrals, and by collisional excitation of the same atomic, molecular, and ionic excited states which are important for cooling the neutral gas. In addition, the electron gas may sometimes be hot enough to collisionally populate excited electronic states of abundant atoms and molecules. The power per area converted into heat in a strong shock is of order $\rho_{n0}V_s^3/2$, where ρ_{n0} is the preshock mass density. At the present time it appears possible to detect H_2 line emission only from shocks with $n_H > 10^4 \text{ cm}^{-3}$.

4 NEW RESEARCH PROBLEMS

In the remainder of this review, I would like to discuss two areas of research which have opened new avenues for the interpretation of interstellar shock waves. The first of these is the topic of unstable or “non-steady shocks”, and the second is the role of thermal conduction in metal-rich shocks associated with “fast-moving knots” in Cas A and other oxygen-rich SNRs.

Since the pioneering work of Cox (1972), most numerical models of radiative shocks have assumed steady flow. However, observations of radiative filaments near some SNRs

(Fesen, Blair, and Kirshner 1982; Hester and Cox 1986) exhibit line ratios which differ from theoretical predictions. These discrepancies may arise because the shock's recombination zone is truncated, because the shocks are unstable, or because the shock flow is not steady. Theoretical considerations which support these interpretations include: (1) the ISM is inhomogeneous on small scales, and some clouds may have columns less than that required ($N_{rec} \approx 10^{19} \text{cm}^{-2}$) for a complete recombination zone; (2) for velocities V_s exceeding 150 to 200 km s^{-1} , the shock front decelerates on a timescale shorter than the time for a parcel of fluid to traverse the radiatively cooling layer; (3) high-velocity shocks may be dynamically unstable.

Several authors have shown that radiative cooling can produce instabilities (Falle 1981; Chevalier and Imamura 1982; Bertschinger 1986). If the logarithmic slope, $\alpha = d(\log \Lambda)/d(\log T)$ is less than a critical value between 0.5 and 1.5, a radiative shock never becomes steady, even if it is driven by a constant-velocity piston. Innes *et al.* (1987b,c) have constructed realistic models of the non-equilibrium ionization and radiative cooling, and conclude that shocks with $V_s > 150 \text{ km s}^{-1}$ are unstable to small perturbations which affect the emission line intensities. There has also been considerable debate about dynamical and gravitational instabilities of shocked gaseous layers (Elmegreen and Lada 1977; Elmegreen and Elmegreen 1978; Vishniac 1983). In recent work, Voit (1987) has shown that in an incompressible fluid, the symmetric and anti-symmetric modes in an unaccelerated slab transform continuously into Rayleigh-Taylor and gravity-wave modes as deceleration becomes more important. Thus, a slab of decelerating gas compressed by a SNR can undergo gravitational collapse and result in accelerated star formation. Even before the slab becomes gravitationally unstable, though, a two-dimensional dynamic instability (Vishniac 1983; Bertschinger 1986) may disrupt the state of the shell. For observers, the key question is whether the non-linear state of the instability is so chaotic that one cannot use idealized models to derive meaningful abundances from the data. I believe that we do not yet have the answer to this question.

A second new area of shock research concerns the role of thermal conduction in metal-rich shocks associated with young SNRs such as Cas A. The fast-moving knots of Cas A (Kirshner and Chevalier 1979) exhibit strong emission lines of oxygen, sulfur, argon, and calcium, but evidently no hydrogen or helium. These emissions have been interpreted as shock-heated gases composed mainly of oxygen (Chevalier and Kirshner 1978, 1979; Itoh 1981). However, these shocks have a number of physical features that make it unwise to extrapolate from cosmic-abundance models:

- For a given velocity, the post-shock temperatures are ~ 16 times greater than cosmic-abundance shocks because of the larger atomic weight of oxygen.
- Heavy-element abundances are enhanced by factors $> 10^3$, resulting in strong radiative cooling, steep temperature gradients, and strong thermal conduction.
- The strong radiative cooling causes temperature decoupling between the ions and electrons, even if $T_e = T_i$ at the front.
- Collisionally excited oxygen lines produce a much stronger photoionizing flux.

Itoh (1981) has computed models of pure-oxygen shocks, neglecting thermal conduction. At $V_s \approx 100 \text{ km s}^{-1}$, the incoming oxygen atoms are mostly preionized by the radiative

precursor. In the post-shock region, the intense radiative cooling results in ion-electron temperature decoupling ($T_e \ll T_i$), and the electron temperature drops to $\sim 10^2 K$ before the ions have a chance to recombine. In these models, one has the amazing result that O IV, O V, and O VI exist at $T \sim 100 K$. However, these models are almost certainly incorrect if one includes the effects of thermal conduction.

In new models of metal-rich shocks, Borkowski and Shull (1987) find that over 90% of the energy flux is carried by thermal conduction. The energy equation (eq. [6]) is modified with a new conductive term but omitting the magnetic field,

$$\frac{d}{dx} \left[\rho v \left(\frac{v^2}{2} + U + \frac{P}{\rho} \right) + \right] + n^2 \mathcal{L}(T) - \frac{d}{dx} \left(\kappa(T) \frac{dT}{dx} \right) = 0. \quad (14)$$

where $\kappa(T) = \kappa_0 T^{5/2}$ is the coefficient of thermal conductivity (Spitzer 1962) and $n^2 \mathcal{L}(T)$ is the total loss function (radiative cooling minus photoelectric heating – see eq. [7]). One can define two scale lengths for cooling and conduction,

$$L_{cool} = \left(\frac{\frac{5}{2} P_s V_s}{n^2 \mathcal{L}(T)} \right); \quad (15)$$

$$L_{cond} = \left(\frac{\kappa(T_s) T_s}{\frac{1}{2} \rho_1 v_1^3} \right), \quad (16)$$

where $v_1 = V_s$ is the shock velocity and P_s and T_s are the post-shock pressure and temperature. The dimensionless ratio of these two lengths, $\alpha = L_{cond}/L_{cool}$ may be used to gauge the importance of conduction. Since $\mathcal{L}(T) \propto \Lambda(T)$ in the absence of heating, $T_s \propto V_s^2$, and $\kappa \propto T^{5/2}$, the parameter $\alpha \propto T_s^{1/2} \Lambda(T_s)$. For temperatures $5.2 < \log T < 7.3$, the radiative cooling coefficient $\Lambda(T) \propto T^{-1/2}$ and α is approximately constant. For normal (cosmic) metal abundances and equilibrium cooling, $\alpha \approx 0.005$ for $V_s \approx 100 \text{ km s}^{-1}$. However, non-equilibrium cooling behind the front can be $\sim 10^2$ times greater than equilibrium values, and oxygen-rich shocks have cooling rates enhanced by over three orders of magnitude. The conclusion is that thermal conduction *must* be included for the Cas A shocks, and it can lead to interesting effects in normal-abundance shocks as well.

Unfortunately, thermal conduction complicates the numerical solution of radiative shocks. Because one must specify not only the post-shock temperature T_s but also the temperature gradient $(dT/dx)_s$, the problem becomes a “two-point boundary value problem”. With special assumptions ($T_i = T_e$, constant ionization fraction, and a specified cooling function), Borkowski and Shull (1987) have separated the second-order energy equation into two integrable equations for $q(T)$ and $T(x)$. A solution yields the conductive flux $q(T) = \kappa(T)(dT/dx)$ in terms of the temperature T , which yields $T(x)$. The conductive flux also affects the Rankine-Hugoniot jump conditions. Figure 3 shows several cosmic-abundance shock solutions for the dimensionless flux $\hat{q} = q(T)/(\frac{1}{2} \rho_1 v_1^3)$ in terms of normalized temperature, $\tau = T/T_{s0}$, where T_{s0} is the post-shock temperature in the absence of conduction. Evidently the effects of conduction are to decrease the post-shock temperature ($\tau < 1$) and flatten the temperature gradients by conducting heat to the cooler post-shock layers. The conductive effects in metal-rich shocks are even more dramatic. Further work is underway, including more realistic non-equilibrium cooling,

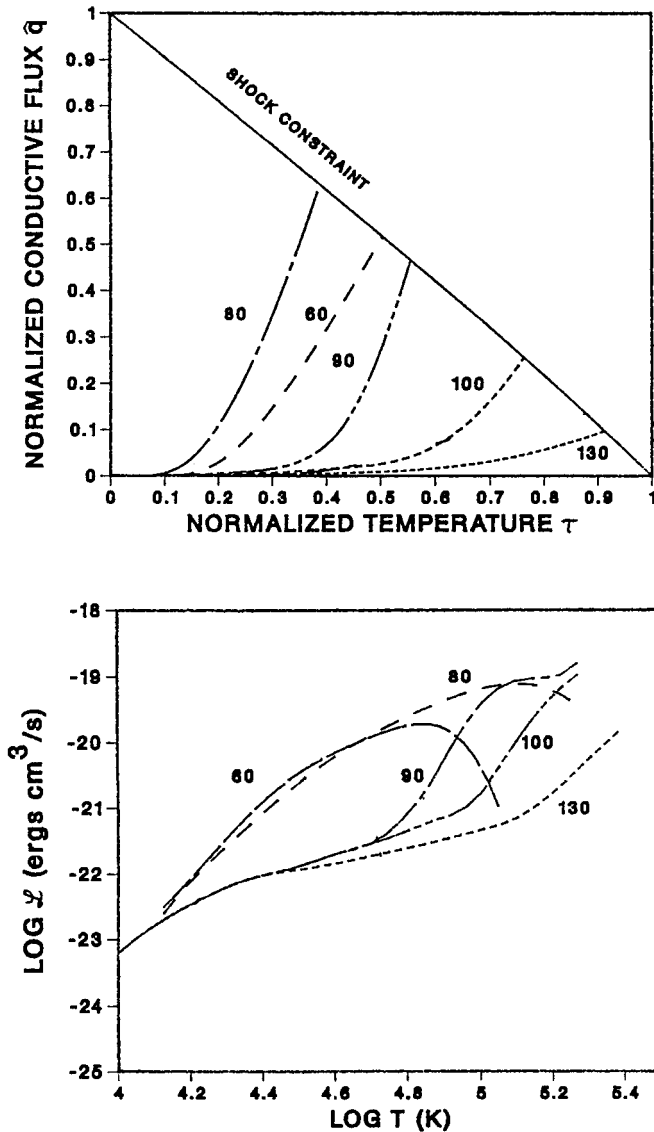


Figure 3: Cosmic-abundance shock trajectories of normalized conductive flux \hat{q} versus normalized temperature $\tau = T/T_{s0}$, based on non-equilibrium cooling rates from Shull and McKee (1979). Shock velocities are given in km s^{-1} . Conductive flux dominates radiative cooling when the trajectory's slope exceeds 45° . The shock constraint represents the front, with conductive effects included in the jump conditions. Clearly, conduction cannot be neglected in the presence of strong non-equilibrium cooling or metallicity enhancements.

ionization, and radiative transfer. The hope is that we will be able use these models to better define the abundances of O, S, Ar, and Ca in these fast-moving knots.

This work was supported by Astrophysical Theory grants from NASA (NSG-7128 and NAG5-193) at the University of Colorado. I thank Dr. Rob Fesen for his comments on the manuscript and Kazimierz Borkowski for discussions on thermal conduction.

REFERENCES

- Baldwin, J.A., Phillips, M.M., and Terlevich, R. 1981, *P.A.S.P.*, **93**, 5.
 Baliunas, S.L., and Butler, S.E. 1980, *Ap. J. Letters*, **235**, L45.
 Barlow, M. 1978, *M.N.R.A.S.*, **183**, 367.
 Becker, R., *et al.* 1979, *Ap. J. Letters*, **234**, L73.
 Becker, R., *et al.* 1980a, *Ap. J. Letters*, **235**, L5.
 ——— 1980b, *Ap. J. Letters*, **237**, L77.
 Bertschinger, E. 1986, *Ap. J.*, **304**, 154.
 Borkowski, K., and Shull, J.M. 1987, in preparation.
 Butler, S.E., and Dalgarno, A. 1980, *Ap. J.*, **241**, 838.
 Butler, S.E., Heil, T.G., and Dalgarno, A. 1980, *Ap. J.*, **241**, 442.
 Butler, S.E., and Raymond, J.C. 1980, *Ap. J.*, **240**, 680.
 Chernoff, D. F. 1987, *Ap. J.*, **312**, 143.
 Chevalier, R.A., and Kirshner, R.P. 1978, *Ap. J.*, **219**, 931.
 Chevalier, R.A., and Kirshner, R.P. 1979, *Ap. J.*, **233**, 154.
 Chevalier, R.A., Kirshner, R.P., and Raymond, J.C. 1980, *Ap. J.*, **235**, 186.
 Chevalier, R.A., and Raymond, J.C. 1978, *Ap. J. Letters*, **225**, L27.
 Clark, R.E.H., Cowan, R.D., and Bobrowicz, F.W. 1986, *Atomic and Nuclear Data Tables*, **34**, 415.
 Cox, D.P. 1972, *Ap. J.*, **178**, 143.
 Cox, D.P., and Raymond, J.C. 1985, *Ap. J.*, **298**, 651.
 Dalgarno, A. 1958, *Phil. Trans. Roy. Soc., Ser. A*, **250**, 426.
 Dalgarno, A., and Butler, S. 1978, *Comments Atom. Molec. Phys.*, **7**, 129.
 Dalgarno, A., Heil, T.G., and Butler, S.E. 1981, *Ap. J.*, **245**, 793.
 Dalgarno, A., and McCray, R. 1972, *Ann. Rev. Astr. Ap.*, **10**, 375.
 Dalgarno, A., and Yadav, H.N. 1953, *Proc. Phys. Soc.*, **A66**, 173.
 Dopita, M., Binette, L., d'Odorico, S., and Benvenuti, P. 1984, *Ap. J.*, **276**, 653.
 Draine, B. T. 1980, *Ap. J.*, **241**, 1021 [Erratum 1981, **246**, 1045].
 Draine, B. T. 1986, *M.N.R.A.S.*, **220**, 133.
 Draine, B. T., Roberge, W. G., and Dalgarno, A. 1983, *Ap. J.*, **264**, 485.
 Draine, B.T., and Salpeter, E.E. 1979, *Ap. J.*, **231**, 77.
 Elmegreen, B.G., and Elmegreen, D.M. 1978, *Ap. J.*, **220**, 1051.
 Elmegreen, B.G., and Lada, C.J. 1977, *Ap. J.*, **214**, 725.
 Fesen, R.A., and Itoh, H. 1985, *Ap. J.*, **295**, 43.

- Fesen, R.A., Blair, W.P., and Kirshner, R.P. 1982, *Ap. J.*, **262**, 171.
 ——— 1985, *Ap. J.*, **292**, 29.
- Gallagher, J., and Pradhan, A.K. 1985, *JILA Information Center Report*, No. 30, University of Colorado.
- Grevesse, N. 1983, *Physica Scripta*, **T8**, 49.
- Gronenschild, E.H.B.M., and Mewe, R. 1982, *Astr. Ap. Suppl.*, **48**, 305.
- Hamilton, A.J.S., Sarazin, C.L., and Chevalier, R.A. 1983, *Ap. J. Suppl.*, **51**, 115.
- Heil, T.G., Butler, S.E., and Dalgarno, A. 1980, *Phys. Rev. A*, **23**, 1100.
- Hester, J.J. 1987, *Ap. J.*, **314**, 181.
- Hester, J.J., and Cox, D.P. 1986, *Ap. J.*, **300**, 675. *Ap. J. Letters*, **252**, L21.
- Hollenbach, D. J., and McKee, C. F. 1979, *Ap. J. Suppl.*, **41**, 555.
 ——— 1980, *Ap. J. Letters.*, **241**, L47.
- Hollenbach, D.J., and Salpeter, E.E. 1971, *Ap. J.*, **163**, 155.
- Innes, D.E., Giddings, J.R., and Falle, S.A.E.G. 1987a, *M.N.R.A.S.*, **224**, 179.
 ——— 1987b, *M.N.R.A.S.*, submitted, *Dynamical Models of Radiative Shocks. II. Unsteady Shocks*.
 ——— 1987c, *M.N.R.A.S.*, submitted *Dynamical Models of Radiative Shocks. II. Spectra*.
- Itoh, H. 1981, *Publ. Astr. Soc. Japan*, **33**, 1.
- Jura, M. 1974, *Ap. J.*, **191**, 375.
- Lepp, S., and Shull, J. M. 1983, *Ap. J.*, **270**, 578.
 ——— 1984, *Ap. J.*, **280**, 465.
- McCarroll, R., and Valiron, P. 1976, *Astr. Ap.*, **53**, 83.
- MacLow, M.M., and Shull, J.M. 1986, *Ap. J.*, **302**, 585.
- McKee, C.F., and Hollenbach, D.J. 1980, *Ann. Rev. Astr. Ap.*, **18**, 219.
- Merts, A.L.; Mann, J.B., Robb, W.D., and Magee, N.W. 1980,
Los Alamos Informal Report No. LA-8267-MS.
- Mouschovias, T. Ch. 1976, *Ap. J.*, **207**, 141.
- Osterbrock, D.E. 1974, *Astrophysics of Gaseous Nebulae*, (San Francisco: Freeman).
- Phillips, A.P., Gondhalekar, P.M., and Pettini, M. 1982, *M.N.R.A.S.*, **200**, 687.
- Raymond, J.C. 1979, *Ap. J. Suppl.*, **39**, 1.
 ——— 1984, *Ann. Rev. Astr. Ap.*, **22**, 75.
- Raymond, J.N., Black, J.H., Dupree, A.K., Hartmann, L.H., and Wolff, R.S. 1981, *Ap. J.*, **246**, 100.
- Raymond, J.N., Blair, W.P., Fesen, R.A., and Gull, T.R. 1983, *Ap. J.*, **275**, 636.
- Raymond, J.C., and Smith, B.W. 1977, *Ap. J. Suppl.*, **35**, 419.
- Reilman, R.F., and Manson, S.T. 1979, *Ap. J. Suppl.*, **40**, 815.
- Roberge, W.G., and Dalgarno, A. 1982, *Ap. J.*, **255**, 176.
- Routly, P.M., and Spitzer, L. 1952, *Ap. J.*, **115**, 227.
- Seab, C.G. 1987, in *Interstellar Processes*, eds. D.J. Hollenbach and H. Thronson, proceedings of Tetons Summer School, (Dordrecht: Reidel), in press.
- Seab, C.G., and Shull, J.M. 1983, *Ap. J.*, **275**, 652.
 ——— 1985, "Shock Processing of Interstellar Grains", in *Interrelationships among Circumstellar, Interstellar, and Interplanetary Grains*, NASA CP-2403, p 37.

- Shapiro, P., and Kang, H. 1987, *Ap. J.*, in press.
- Shull, J.M. 1978, *Ap. J.*, **219**, 877.
- 1981, *Ap. J. Suppl.*, **46**, 27.
- 1982, *Ap. J.*, **262**, 308.
- Shull, J.M., and Beckwith, S. 1982, *Ann. Rev. Astr. Ap.*, **20**, 163.
- Shull, J.M., and Draine, B.T. 1987, in *Interstellar Processes*, eds. D.J. Hollenbach and H. Thronson, proceedings of Tetons Summer School, (Dordrecht: Reidel), in press.
- Shull, J.M., and McKee, C.F. 1979, *Ap. J.*, **227**, 131.
- Shull, J.M., and Van Steenberg, M.E. 1982, *Ap. J. Suppl.*, **48**, 95 [Erratum **49**, 351].
- Shull, J.M., York, D.G., and Hobbs, L.M. 1977, *Ap. J. Letters*, **211**, L139.
- Siluk, R., and Silk, J. 1974, *Ap. J.*, **192**, 51.
- Spitzer, L. 1962, *Physics of Fully Ionized Gases* (2d ed.; New York: Interscience) *Ann. Rev. Astr. Ap.*, **13**, 133.
- Troland, T. H., and Heiles, C. 1986, *Ap. J.*, **301**, 339.
- Turner, J., Kirby-Docken, K., and Dalgarno, A. 1977, *Ap. J. Suppl.*, **35**, 281.
- van Dishoeck, E.F., and Black, J.H. 1986, *Ap. J. Suppl.*, **62**, 109.
- Van Steenberg, M.E., and Shull, J.M. 1987, *Ap. J.*, in press.
- Vishniac, E.T. 1983, *Ap. J.*, **274**, 152.
- Voit, G.M. 1987, this conference (and *Ap. J.*, in preparation).
- Withbroe, G. 1971, in "The Menzel Symposium", NBS SP-53, ed. K. Gebbie, (Washington: Government Printing Office).